

Improvement of Analysis for Relaxation of Fluctuations by Using Gaussian Process Regression and Extrapolation Method

Yuma Osada* and Yukiyasu Ozeki

Department of Engineering Science,

Graduate School of Informatics and Engineering,

The University of Electro-Communications,

1-5-1 Chofugaoka, Chofu-shi, Tokyo 182-8585, Japan

(Dated: September 30, 2024)

Abstract

The nonequilibrium relaxation (NER) method, which has been used to investigate equilibrium phase transitions via their nonequilibrium behavior, has been widely applied to various models to estimate critical temperatures and critical exponents. Although the estimation of critical temperatures has become more reliable and reproducible, that of critical exponents raises concerns about the method's reliability. Therefore, we propose a more reliable and reproducible approach using Gaussian process regression. In addition, the present approach introduces statistical errors through the bootstrap method by combining them using the extrapolation method. Our estimation for the two-dimensional Ising model yielded $\beta = 0.12504(6)$, $\gamma = 1.7505(10)$, and $\nu = 1.0003(6)$, which are consistent with the exact values. The value $z = 2.1669(9)$ is reliable because of the high accuracy of these exponents. We also obtained the critical exponents for the three-dimensional Ising model and found that they are close to those reported in a previous study. Thus, for systems undergoing second-order transitions, our approach improves the accuracy, reliability, and reproducibility of the NER analysis. Because the proposed approach requires the relaxation of some observables from Monte Carlo simulations, its simplicity imparts it with significant potential.

I. Introduction

Critical exponents are essential for understanding critical universality. Various methods for estimating critical exponents have been developed, including nonequilibrium relaxation (NER) analysis,^{1–3} finite-size scaling analysis,^{4,5} conformal-bootstrap theory,⁶ and the tensor-renormalization group method.⁷ The NER method is used to analyze the properties of a system’s equilibrium state on the basis of its nonequilibrium behavior. It has been applied to various systems. In particular, it has been used to analyze slow-relaxing systems, such as those undergoing critical slowing down. Examples include systems that undergo the Kosterlitz–Thouless^{8–11} transition,^{3,12} spin-glass systems,^{1,13,14} and fully frustrated systems.^{15,16} In addition, the scheme of the NER method has been applied to a transition in the percolation model.⁷ Thus, the NER analysis is applicable to numerous models and contributes to research on phase transitions and critical phenomena.

The difficulty in the NER analysis of fluctuations lies in calculating the differentiation of discrete values obtained from a simulation. In the NER analysis of fluctuations, critical exponents are derived from the slope of the data values. For the NER method, in contrast to the well-established dynamical scaling analysis for critical temperatures,¹⁷ a stable and automatic analysis to determine critical exponents has not yet been developed. There are two primary issues with the conventional method used in this analysis. The first issue is the unstable nature of the slopes produced by the conventional method. Simple numerical differentiation is ineffective because of the noise present in the data. For the conventional method, efforts have been made to reduce the effect of noise using a linear approximation to determine the slope. However, the instability still needs to be addressed and the reliability of the analysis must be determined. The second issue is the difficulty in determining the convergence behavior from discontinuous and non-monotonic values when extrapolating to estimate critical exponents. In the conventional method, the form of the slope is assumed to be $a_1(1/t)^{a_2} + a_3$, which emphasizes the short-time behavior. Note that the time t is measured in a unit of Monte Carlo steps (MCSs) in simulations. For example, the interval $t = [1, 10]$ corresponds to $1/t = [0.1, 1]$, which is 90% of the interval $1/t = [0, 1]$ ($t = [1, \infty]$). These drawbacks undermine the reliability of extrapolations to the thermodynamic limit as $t \rightarrow \infty$. To overcome these issues, we use Gaussian process regression for the continuous slope. Selecting an appropriate extrapolation method based on this continuous slope is

critical.

Through this work, we aim to enhance the reliability and reproducibility of analyses by offering a systematic approach to the NER analysis of fluctuations. We demonstrate the utility of the present method using two systems. In the two-dimensional square Ising model, we validate our approach by comparing the critical exponents obtained at the exact critical temperature. In the three-dimensional cubic Ising model, where the exact critical temperature remains unknown, we demonstrate the applicability of the present method near the critical temperature through comparisons with previous studies.

The remainder of this paper is organized as follows: In Sect. II, we explain the NER method of fluctuation. In Sect. III, we propose an improved analysis and validate our approach at the exact critical temperature using the two-dimensional Ising model. In Sect. IV, we apply the present method to the three-dimensional Ising model and justify it by comparing the results with those obtained using the methods reported in previous studies. In Sect. V, we summarize the present study and the proposed method.

II. Estimation of Critical Exponents Using Nonequilibrium Relaxation of Magnetization and Fluctuations

Let us explain how to use NER data to estimate the critical exponents β , γ , ν , and z of systems that undergo a second-order transition. In the NER analysis, we simulate a large system considered to have no finite-size effects in the observed time interval. We use

$$m(t) \equiv \frac{1}{N_{\text{size}}} \sum_i s_i(t) \quad (1)$$

as the dynamical order parameter at time t , where s_i is ± 1 and N_{size} denotes the number of spins. Hereafter, we measure the time t in simulations in a unit of MCSs. The simulation aims to calculate relaxations of some quantities numerically, including the order parameter $m(t)$ and its fluctuations, which asymptotically exhibit algebraic behavior with respect to time t at the critical temperature;³ *e.g.*, the relaxation of magnetization $m(t)$ from the all-up state shows an algebraic behavior, $m(t) \sim t^{-\beta/(z\nu)}$. To observe the asymptotic power clearly from the estimated numerical data up to a finite maximum time, the local exponent of magnetization λ_m defined by

$$\lambda_m(t) \equiv -\frac{\partial \log m(t)}{\partial \log t} \rightarrow \frac{\beta}{z\nu} \quad (2)$$

is useful. This local exponent is also useful in estimating critical temperatures because the asymptotic behavior of magnetization is represented by

$$m(t) \sim \begin{cases} \exp(-t/\tau) & T > T_C, \\ t^{-\beta/(z\nu)} & T = T_C, \\ m_{\text{eq}} & T < T_C, \end{cases} \quad (3)$$

where τ is the relaxation time. Although we can determine the range of critical temperatures from the relaxation of $\lambda_m(t)$, which is called pinching estimation, we do not estimate critical temperatures in this study because we use the exact critical temperature for the two-dimensional Ising model and the highly accurate critical temperature obtained from massive calculations in the previous NER analysis reported by Ito¹⁸ for the three-dimensional Ising model. The relaxation of fluctuations, which asymptotically exhibits algebraic behavior with respect to time t at the critical temperature, is defined as

$$\begin{aligned} \chi(t) &\equiv \langle m(t)^2 \rangle - \langle m(t) \rangle^2 \sim t^{\gamma/(z\nu)} \\ \partial m(t) &\equiv |\langle m(t)e(t) \rangle - \langle m(t) \rangle \langle e(t) \rangle| \sim t^{(1-\beta)/(z\nu)}, \end{aligned} \quad (4)$$

where $\langle \cdot \rangle$ denotes the dynamical average and $e(t)$ represents the internal energy per site. Note that we use variance fluctuations in the present paper, instead of the dimensionless fluctuations that have been used in previous NER studies,³ because they enable easier calculation of errors of fluctuations. The present method can be used for either variance fluctuations or dimensionless fluctuations, and the accuracy does not appear to change for either. Their local exponents are also defined as

$$\begin{aligned} \lambda_\chi(t) &\equiv \frac{\partial \log \chi(t)}{\partial \log t} \rightarrow \frac{\gamma}{z\nu} \\ \lambda_{\partial m}(t) &\equiv \frac{\partial \log \partial m(t)}{\partial \log t} \rightarrow \frac{1-\beta}{z\nu}. \end{aligned} \quad (5)$$

From combinations of these local exponents, we can derive functions that asymptotically approach critical exponents:

$$\begin{aligned} \beta &= \lim_{t \rightarrow \infty} \beta(t) = \lim_{t \rightarrow \infty} \frac{\lambda_m(t)}{\lambda_{\partial m}(t) + \lambda_m(t)} \\ \gamma &= \lim_{t \rightarrow \infty} \gamma(t) = \lim_{t \rightarrow \infty} \frac{\lambda_\chi(t)}{\lambda_{\partial m}(t) + \lambda_m(t)} \\ \nu &= \lim_{t \rightarrow \infty} \nu(t) = \lim_{t \rightarrow \infty} \frac{2\lambda_m(t) + \lambda_\chi(t)}{d(\lambda_{\partial m}(t) + \lambda_m(t))} \\ z &= \lim_{t \rightarrow \infty} z(t) = \lim_{t \rightarrow \infty} \frac{1}{\nu(\lambda_{\partial m}(t) + \lambda_m(t))}, \end{aligned} \quad (6)$$

where d denotes the dimension of the system. Consequently, we can estimate critical exponents by simulating $m(t)$, $\chi(t)$, and $\partial m(t)$ at the critical temperature, differentiating them on a double-logarithmic scale, and extrapolating their combinations.

III. Improvement through Gaussian Process Regression

A. Using Gaussian process regression

Let us first explain how to obtain local exponents in Eqs. (2) and (5) by differentiating values on a double-logarithmic scale. In contrast to numerical differentiation, Gaussian process regression enables us to obtain analytic and continuous derivatives.^{19–21} We here briefly explain this process. We aim to obtain the regression function for N_{data} data points (X_i, Y_i, E_i) , where i is the label for data, X_i is an explanatory variable for Y_i , and E_i represents the error in Y_i for $i = 1, \dots, N_{\text{data}}$. We maximize the log-likelihood function by optimizing hyperparameters $\boldsymbol{\theta}$. The log-likelihood function for a Gaussian process is defined as

$$\log L(\boldsymbol{\theta}) = -\frac{1}{2} \log |\Sigma(\boldsymbol{\theta})| - \frac{1}{2} \mathbf{Y}^T \Sigma(\boldsymbol{\theta})^{-1} \mathbf{Y} - \frac{N}{2} \log(2\pi), \quad (7)$$

where $\Sigma(\boldsymbol{\theta})$ is the $N_{\text{data}} \times N_{\text{data}}$ variance-covariance matrix and $|\Sigma|$ denotes the determinant of Σ . Element (i, j) of Σ is defined by

$$\Sigma_{ij}(\boldsymbol{\theta}) = E_i^2 \delta_{ij} + K(X_i, X_j, \boldsymbol{\theta}), \quad (8)$$

where $K(X_i, X_j, \boldsymbol{\theta})$ is a kernel function. In Gaussian process regression, assuming all data points obey a multivariate Gaussian distribution, we can predict new points assumed to follow that distribution. Specifically, we can predict Y at X using optimized hyperparameters $\boldsymbol{\theta}_{\text{opt}}$ as

$$Y_{\text{predict}}(X) = \mathbf{k}^T \Sigma(\boldsymbol{\theta}_{\text{opt}})^{-1} \mathbf{Y}, \quad (9)$$

where $\mathbf{k} = (k_i)$, $k_i(X) = K(X_i, X, \boldsymbol{\theta}_{\text{opt}})$, and Y_{predict} is the prediction function for Y . We can analytically obtain the derivative of Y by

$$\frac{\partial Y_{\text{predict}}(X)}{\partial X} = \left(\frac{\partial \mathbf{k}^T}{\partial X} \right) \Sigma(\boldsymbol{\theta}_{\text{opt}})^{-1} \mathbf{Y}. \quad (10)$$

In the following discussion, we demonstrate how to estimate critical exponents using the two-dimensional square Ising model. The dynamical order parameter for this model,

the magnetization $m(t)$, is calculated as $m(t) = N_{\text{size}}^{-1} \sum_i s_i(t)$, starting from the all-up state. We analyze data pairs t_i versus y_i ($= 1/m_i, \chi_i$, or ∂m_i) to apply Gaussian process regression for differentiation. In this paper, we use a composition kernel function consisting of a Gaussian kernel K_G and a constant kernel K_C , represented by

$$\begin{aligned} K_G(X_i, X_j, \{\theta_1, \theta_2\}) &= \theta_1^2 \exp\left(-\frac{(X_i - X_j)^2}{2\theta_2^2}\right) \\ K_C(X_i, X_j, \{\theta_3\}) &= \theta_3^2 \\ K(X_i, X_j, \boldsymbol{\theta}) &= K_G(X_i, X_j, \{\theta_1, \theta_2\}) + K_C(X_i, X_j, \{\theta_3\}), \end{aligned} \tag{11}$$

where θ_1, θ_2 , and θ_3 are hyperparameters. This kernel is generally used in Gaussian process regression. The Gaussian kernel function ensures smoothness and locality, whereas the constant kernel contributes to the global behavior. (Although we initially used the polynomial kernel function under the assumption that local exponents are monotonic, we realized that they are not monotonic after applying this approach.) For the stability of the regression, we convert the obtained data as

$$\begin{aligned} X_i &\equiv \frac{1}{\log(t_i) + c_x} \\ Y_i &\equiv \frac{1}{c_{y1} \log(y_i) + c_{y2}} \\ E_i &\equiv \frac{c_{y1} e_{y_i}}{y_i (c_{y1} \log(y_i) + c_{y2})^2} \\ c_x &\equiv 1 - \min_i \{\log(t_i)\} \\ c_{y1} &\equiv \frac{\max_i \{\log(t_i)\} - \min_i \{\log(t_i)\}}{\max_i \{\log(y_i)\} - \min_i \{\log(y_i)\}} \\ c_{y2} &\equiv 1 - c_{y1} \min_i \{\log(y_i)\}, \end{aligned} \tag{12}$$

where e_i represents the error in y_i and c_x , c_{y1} , and c_{y2} are constants determined by the data. Note that the condition $0 \leq X_i, Y_i \leq 1$ is satisfied, corresponding to normalization in machine learning. This conversion remains invariant even if y_i is multiplied by a positive constant value, and it makes X_i and Y_i dimensionless quantities. In the thermodynamic limit, $y \rightarrow \infty$ as $t \rightarrow \infty$ must be observed at the critical temperature for each case of $y = 1/m, \chi, \partial m$. Therefore, we include the data point $(X_i, Y_i, E_i) = (0, 0, 0)$ for the regressions of each case. The local exponent at $X = 1/(\log(t) + c_x)$ is represented by Eqs. (9) and (10)

as

$$\begin{aligned}
\lambda_y(t) &= \frac{\partial \log(y)}{\partial \log(t)} \\
&= \frac{\partial \log(y)}{\partial Y} \frac{\partial X}{\partial \log(t)} \frac{\partial Y}{\partial X} \\
&= \frac{X^2}{c_{y1} Y^2} \frac{\partial Y}{\partial X} \\
&= \frac{X^2}{c_{y1} (Y_{\text{predict}}(X))^2} \frac{\partial Y_{\text{predict}}(X)}{\partial X} \\
\frac{\partial X}{\partial \log(t)} &= -\frac{1}{(\log(t) + c_x)^2} = -X^2 \\
\frac{\partial Y}{\partial \log(y)} &= -\frac{c_{y1}}{(c_{y1} \log(y) + c_{y2})^2} = -c_{y1} Y^2.
\end{aligned} \tag{13}$$

Note that, in contrast to the numerical differentiation, the present method enables us to obtain Y and $\frac{\partial Y}{\partial X}$ at t as Y_{predict} and $\frac{\partial Y_{\text{predict}}}{\partial X}$, respectively. Therefore, we can predict local exponents $\beta(t)$, $\gamma(t)$, $\nu(t)$, and $z(t)$ from Eqs. (6) and (13). Although we might be able to compute the exponent $\alpha(t)$ directly from the relaxation of specific heat,³ we did not calculate it in the present work because of its slow convergence. Estimating $\alpha(t)$ with the same accuracy as other critical exponents in the same observation time has long been considered difficult. Of course, we can calculate α using the scaling relation.

B. Demonstration for the two-dimensional Ising model

Hereafter, measured temperatures are reported in units of J/k_B . We conducted simulations using the Metropolis algorithm on a $N_{\text{size}} = 501 \times 500$ square lattice with skew boundary conditions at the critical temperature $T = T_C = 2.26918531421$. An observation consists of 10^4 MCSs, with statistical averaging over 10,137,600 independent samples. Initially, in NER analysis, we examine size dependence. The overlapping error bars shown in Fig. 1 indicate that the finite-size effect is negligible on a $N_{\text{size}} = 501 \times 500$ lattice up to 10^4 MCSs.

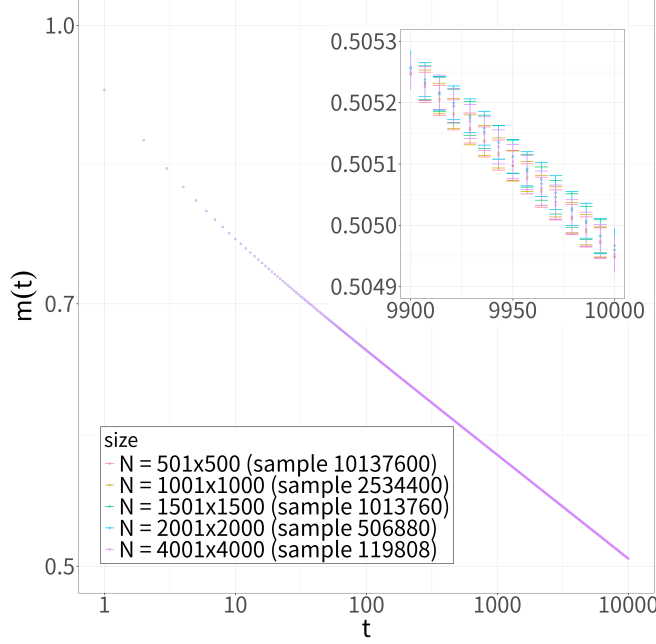


FIG. 1. (Color Online) Size dependence of the relaxation of $m(t)$ from the all-up state for the two-dimensional Ising model, plotted on a double-logarithmic scale for $1 \leq t \leq 10,000$ at the critical temperature $T = 2.26918531421 = T_C$. The inset gives $m(t)$ between $t = 9900$ and $10,000$. The overlapping error bars for each lattice size suggest negligible size dependence for the $N_{\text{size}} = 501 \times 500$ lattice up to 10^4 MCSs.

Thus, we applied the present method using simulations with the $N_{\text{size}} = 501 \times 500$ lattice to estimate local exponents. For the regression analysis, we extracted $N_{\text{data}} = 100$ data points at equal intervals of $\log(t)$ from the simulation data, ranging from $t = 10$ to $t = 10,000$. The results of the Gaussian process regression based on Eq. (12) are shown in Figs. 2 to 4.

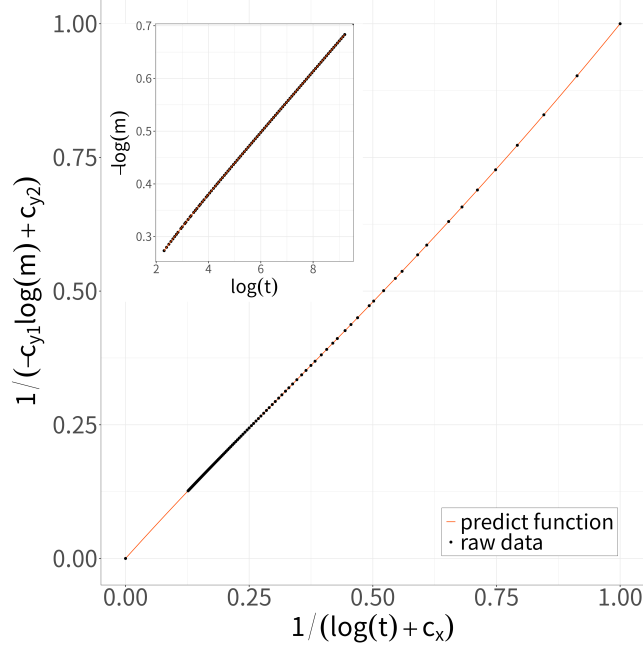


FIG. 2. (Color Online) Regression of $X = 1/(\log(t) + c_x)$ vs $Y = 1/(-c_{y1} \log(m) + c_{y2})$ for the two-dimensional Ising model, within the bounds $0 \leq X, Y \leq 1$. Black closed circles represent raw data points from the simulation, and the orange line depicts the interpolation. The inset shows the raw data of $\log(t)$ vs $-\log(m)$ and their prediction.

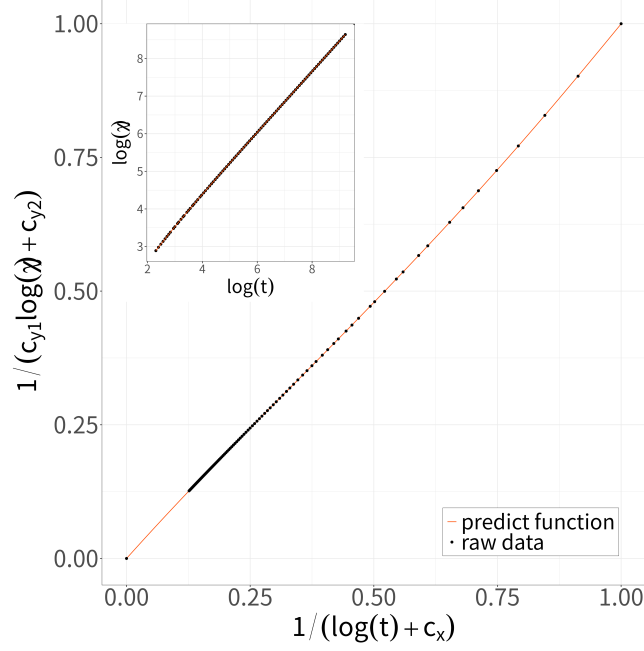


FIG. 3. (Color Online) Regression of $X = 1/(\log(t) + c_x)$ vs $Y = 1/(c_{y1}\log(\chi) + c_{y2})$ for the two-dimensional Ising model, within the bounds $0 \leq X, Y \leq 1$. Black closed circles represent raw data points from the simulation, and the orange line depicts the interpolation. The inset shows the raw data of $\log(t)$ vs $\log(\chi)$ and their prediction.

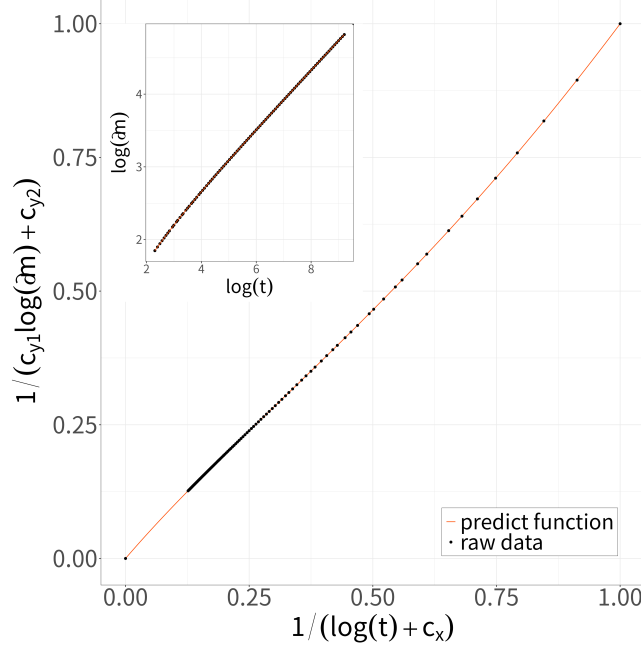


FIG. 4. (Color Online) Regression of $X = 1/(\log(t) + c_x)$ vs $Y = 1/(c_{y1} \log(\partial m) + c_{y2})$ for the two-dimensional Ising model, within the bounds $0 \leq X, Y \leq 1$. Black closed circles represent raw data points from the simulation, and the orange line depicts the interpolation. The inset shows the raw data of $\log(t)$ vs $\log(\partial m)$ and their prediction.

Figures 5 to 8 display the local exponents in the observed time interval, as estimated using Eqs. (6) and (13). We plotted $N = 1003$ data points at equal intervals of t in these figures. In contrast to numerical differentiation, our approach predicts derivatives at specific times. Note that we predict and use values in the observed time interval $10 \leq t \leq 10,000$ because predictions outside this interval are unstable. If we use an interval around $(X, Y) = (0, 0)$ for the interpolation by regression, the value of $\frac{X^2}{Y_{\text{predict}}^2}$ in Eq. (13) close to that interval is also unstable because of the small values in the fraction.

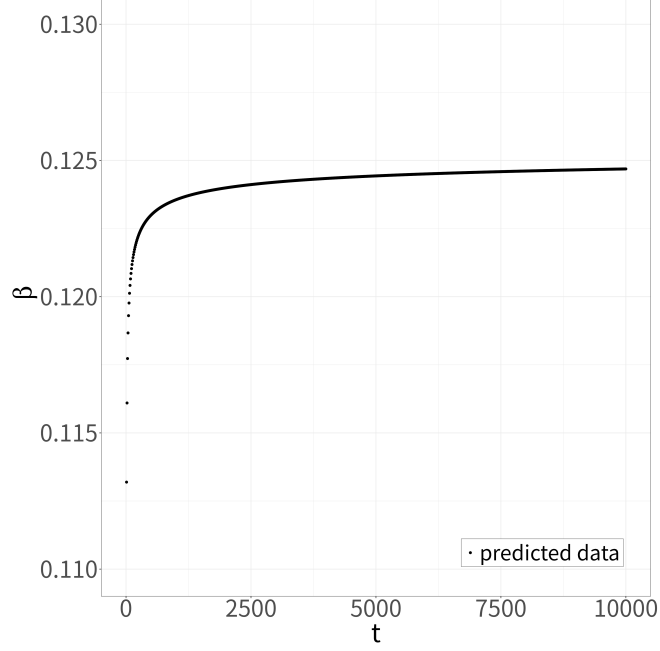


FIG. 5. Interpolation of t vs β for the two-dimensional Ising model. Black closed circles represent interpolated values at equal intervals of t .

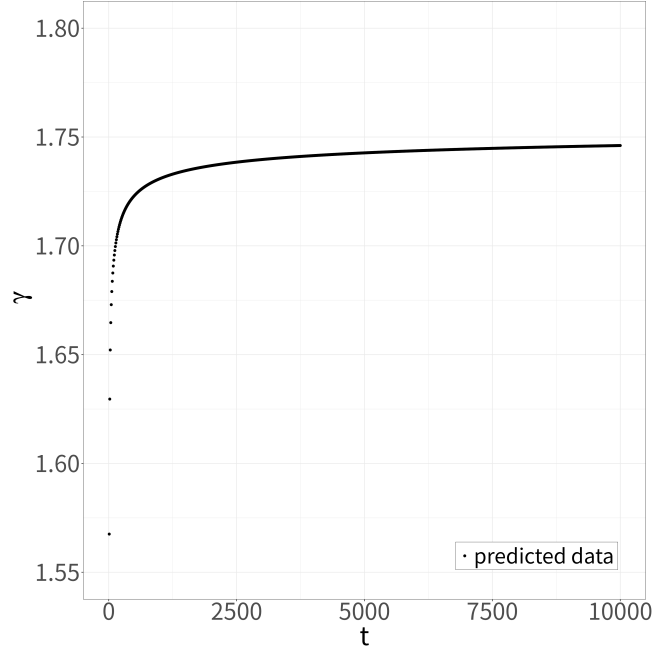


FIG. 6. Interpolation of t vs γ for the two-dimensional Ising model. Black closed circles represent interpolated values at equal intervals of t .

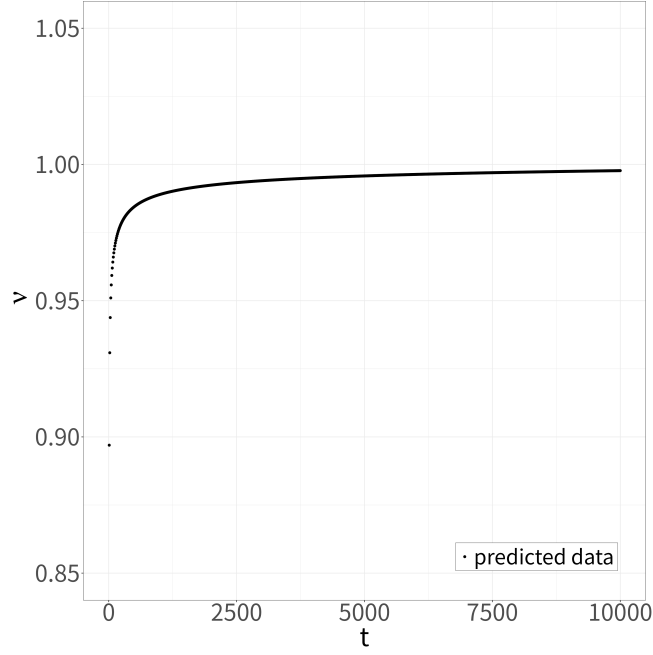


FIG. 7. Interpolation of t vs ν for the two-dimensional Ising model. Black closed circles represent interpolated values at equal intervals of t .

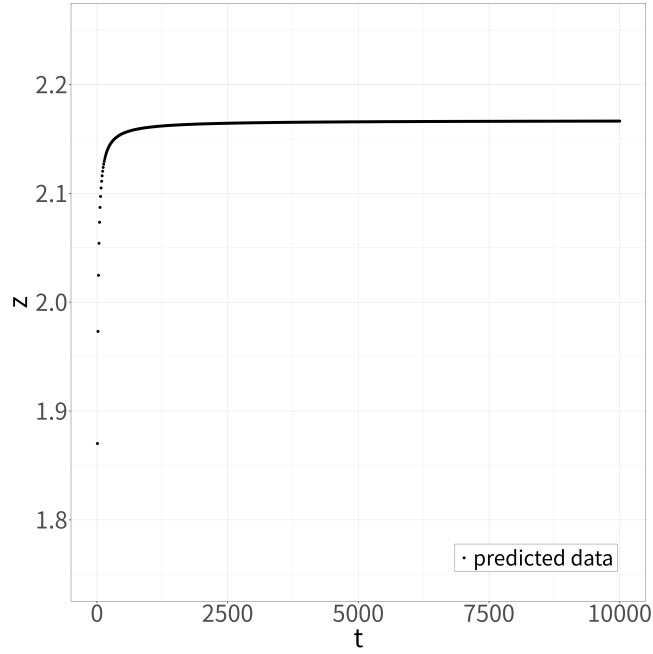


FIG. 8. Interpolation of t vs z for the two-dimensional Ising model. Black closed circles represent interpolated values at equal intervals of t .

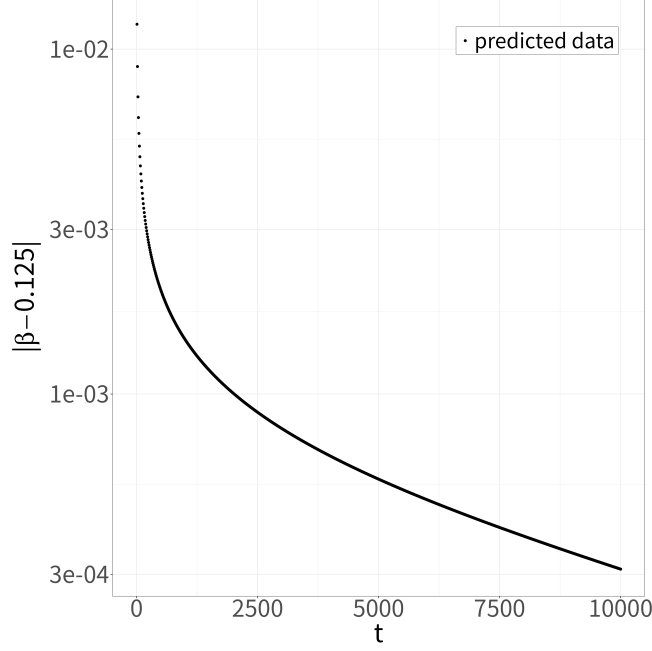


FIG. 9. Interpolation of t vs $|\beta - 0.125|$ for the two-dimensional Ising model, plotted on a semilogarithmic graph with the y-axis on a logarithmic scale. Black closed circles represent interpolated values at equal intervals of t .

Finally, we apply the extrapolation method for systematicity and reproducibility to estimate critical exponents as $t \rightarrow \infty$. We use the ε -algorithm,^{22–24} which is an efficient implementation of the Shanks transformation.²⁵ Briefly, the Shanks transformation extrapolates sequences that converge exponentially. In Fig. 9, we replotted $\beta(t)$ shown in Fig. 5 in order to see the exponential convergence in the asymptotic region. Thus we assume that local exponents such as $\beta(t)$ converge exponentially with respect to t ; hereafter, we apply the ε -algorithm to the sequences obtained from regressions. Now we define the sequence v_s as

$$v_s \equiv v \left(\frac{(N-1-s)t_{\min} + st_{\max}}{N-1} \right), \quad s = 0, \dots, N-1 \quad (14)$$

where s is the label for data, $t_{\min}(t_{\max})$ is the minimum (maximum) time in the interval, N denotes the number of data, and $v(t)$ represents $\beta(t)$, $\gamma(t)$, $\nu(t)$, or $z(t)$. The ε -algorithm progresses as follows:

$$\frac{1}{\varepsilon_{s-1,k+1} - \varepsilon_{s,k}} + \frac{1}{\varepsilon_{s+1,k-1} - \varepsilon_{s,k}} = \frac{1}{\varepsilon_{s-1,k} - \varepsilon_{s,k}} + \frac{1}{\varepsilon_{s+1,k} - \varepsilon_{s,k}}, \quad s, k = 0, 1, \dots, \quad (15)$$

starting with $\varepsilon_{s,-1} = \infty$, and $\varepsilon_{s,0} = v_s$ for $s = 0, \dots, N-1$. We can obtain the convergence-accelerated sequence $\varepsilon_{s,k}$ by applying the transformation k times, where the length is $N-2k$.

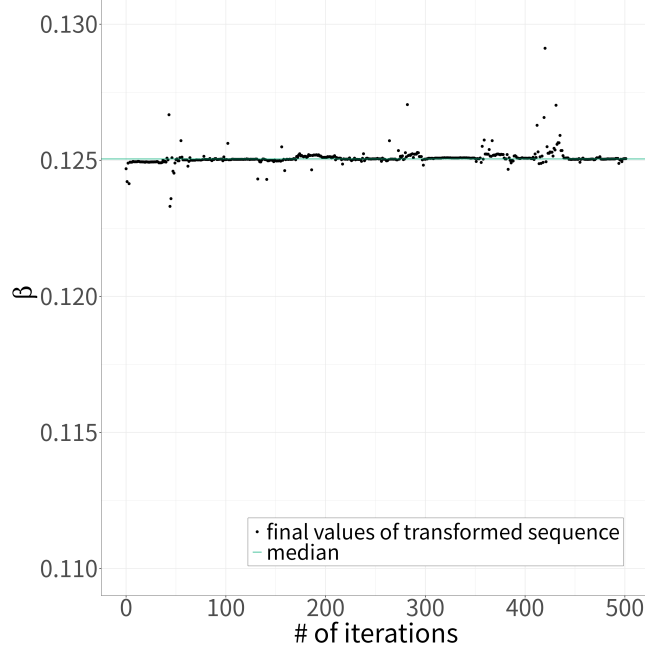


FIG. 10. (Color Online) Extrapolation of the number of iterations k vs β for the two-dimensional Ising model with the length of the original sequence $N = 1003$. Black closed circles represent the final values of the transformed sequence. The green line represents their median.

In the present study, we estimate the critical exponent by taking the median of the final values in the extrapolated sequence $\varepsilon_{s,k}$ for $k = 0, \dots, \lfloor (N-1)/2 \rfloor$, with $N = 1003$ data points at equal intervals of t . Specifically, we calculate the limit V using

$$V = \text{median}(\{v_{k,\text{final}} \mid v_{k,\text{final}} = \varepsilon_{N-1-2k,k}, k = 0, \dots, \lfloor (N-1)/2 \rfloor\}) \quad (16)$$

as the estimator of the critical exponent. Note that we opted to use the median and $N = 1003$ interpolated data to mitigate the effect of outliers given that the actual data sequence may not perfectly adhere to Eq. (15) because of numerical errors. Because most of the final values shown in Fig. 10 are close to the median, we regard the median as the limit to neglect outliers. We obtain $\beta = 0.12507\dots$, $\gamma = 1.7508\dots$, $\nu = 1.0004\dots$, and $z = 2.1668\dots$, which closely approximate the exact values $\beta = 0.125$, $\gamma = 1.75$, and $\nu = 1$ and are consistent with previously reported results $z = 2.1667(5)$.²⁶

Because the present method operates automatically, reproducibly, and reliably, we can easily apply the bootstrap method.²⁷ We created 100 bootstrap samples by resampling $N_{\text{data}} = 100$ data points, extracted at equal intervals of $\log(t)$, 100 times. We indepen-

TABLE I. Critical exponents for the two-dimensional Ising model from various studies.

Reference	Method	β	γ	ν	z
Exact values		0.125	1.75	1	
Nightingale <i>et al.</i> (2000) ²⁶	MC				2.1667(5)
Adzhemyan <i>et al.</i> (2022) ²⁸	ε expansion				2.14(2)
Our results ($10 \leq t \leq 1000$)	NER	0.1241(1)	1.7364(14)	0.9923(8)	2.1719(5)
Our results ($10 \leq t \leq 5000$)	NER	0.12473(6)	1.7438(9)	0.9966(5)	2.1715(9)
Our results ($10 \leq t \leq 10,000$)	NER	0.12504(6)	1.7505(10)	1.0003(6)	2.1669(9)

dently applied the present method to each bootstrap sample and estimated the mean and numerical errors of the critical exponents across the bootstrap samples. Consequently, we estimated the critical exponents as $\beta = 0.12504(6)$, $\gamma = 1.7505(10)$, and $\nu = 1.0003(6)$, which are consistent with the exact values $\beta = 0.125$, $\gamma = 1.75$, and $\nu = 1$. The value $z = 2.1669(9)$ is reliable because of the high accuracy of these exponents. Our estimation of the dynamical exponent $z = 2.1669(9)$ is consistent with that reported in a previous study [$z = 2.1667(5)$]²⁶ and is close to that reported in another study [$z = 2.14(2)$].²⁸

We also applied the present method to the same model over various time intervals. The results are shown in Table I. As the upper time interval increases, the estimation accuracy for critical exponents improves and the exponents become consistent with the exact values and with the results of the previous study.²⁶ These results validate the accuracy and reliability of the present method at the critical temperature and demonstrate the sufficiency of the interval $t = [10, 10,000]$. Data from a simple simulation for the relaxation of the appropriate quantities enable us to derive highly reliable critical exponents.

C. Advantage over the conventional method

Because we have numerically demonstrated that the present method is reliable, we also illustrate the improvement visually. In the conventional method, we compute λ_m from a linear approximation of sections. The controllable conditions are the number of averages

N_{ave} and the choice of sections. Therefore, we calculate λ_m at $t = (t_l + t_r)/2$ as

$$\lambda_m \left(\frac{t_l + t_r}{2} \right) = (\text{slope of } -\log(m) \text{ over } [t_l, t_r]),$$

where data points lie at equal intervals in t , both t_l and t_r are integers, and $t_r - t_l + 1 = N_{\text{ave}}$. In contrast to the conventional method, the controllable condition for the present method is the time interval for the regression. Figure 11 shows a plot of λ_m values obtained under several controllable conditions using the conventional method as well as those obtained using the improved method. The data points for both methods exhibit similar trends. Although the data points for the conventional method are sensitive to the number of averages, those for the present method are less affected by the choice of the regression interval. This plot indicates that the present method has improved reliability compared with the conventional method and overcomes discreteness.

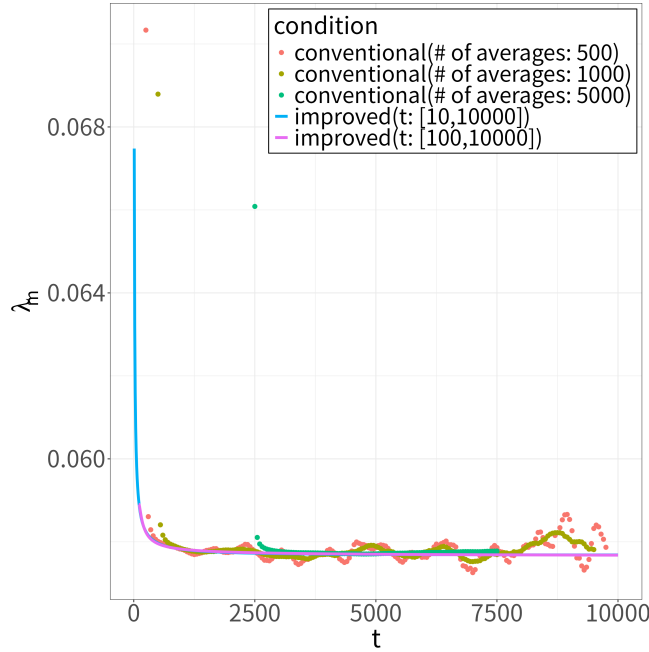


FIG. 11. (Color Online) λ_m obtained using the conventional method and that obtained using the improved method. Circles represent the values obtained using the conventional method for several average numbers. Lines represent the values obtained using the improved method for several regression intervals. For the conventional method, the data points lie at equal intervals of t in increments of 50.

IV. Application to the Three-dimensional Ising Model

Because the analysis for the two-dimensional Ising model at the exact critical temperature was successful, we applied the proposed method to the three-dimensional cubic Ising model, whose exact transition temperature is unknown. We conducted analyses of this model at the temperature $T = 1/0.2216547 = 4.51152174982078$. This temperature was estimated in a previous study using the pinching estimation of the NER method¹⁸ explained in Sect. II. Simulations were performed on a $N_{\text{size}} = 201 \times 201 \times 200$ cubic lattice with skew boundary conditions at $T = 4.51152174982078$. Observations consisted of 10^3 MCSs, with statistical averaging over 1,244,160 independent samples. The overlapping error bars shown in Fig. 12 indicate that the finite-size effect is negligible on a $N_{\text{size}} = 201 \times 201 \times 200$ lattice up to 10^3 MCSs.

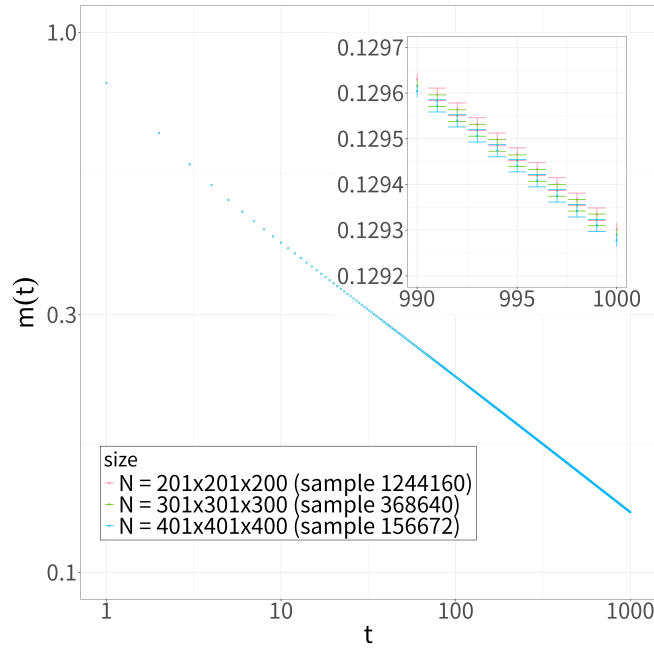


FIG. 12. (Color Online) Size dependence of the relaxation of $m(t)$ from the all-up state for the three-dimensional Ising model, plotted on a double-logarithmic scale for $1 \leq t \leq 1000$ at temperature $T = 4.51152174982078 \simeq T_C$. The inset illustrates $m(t)$ between $t = 990$ and 1000 . The overlapping error bars for each lattice size suggest negligible size dependence for the $N_{\text{size}} = 201 \times 201 \times 200$ lattice up to 10^3 MCSs.

Similar to the above analysis, we applied the proposed method to the three-dimensional Ising model. The regressions are shown in Figs. 13 to 15.

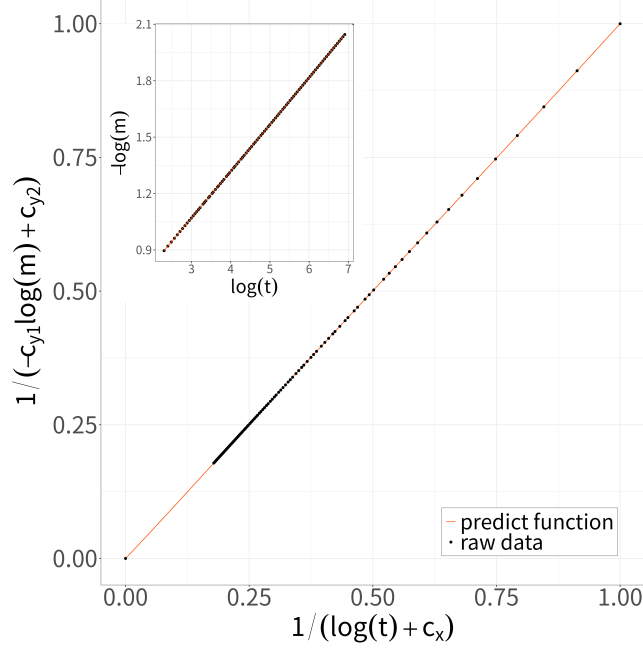


FIG. 13. (Color Online) Regression of $X = 1/(\log(t) + c_x)$ vs $Y = 1/(-c_{y1}\log(m) + c_{y2})$ for the three-dimensional Ising model, within the bounds $0 \leq X, Y \leq 1$. Black closed circles represent raw data points from the simulation; the orange line depicts the interpolation. The inset shows the raw data of $\log(t)$ vs $-\log(m)$ and their prediction.

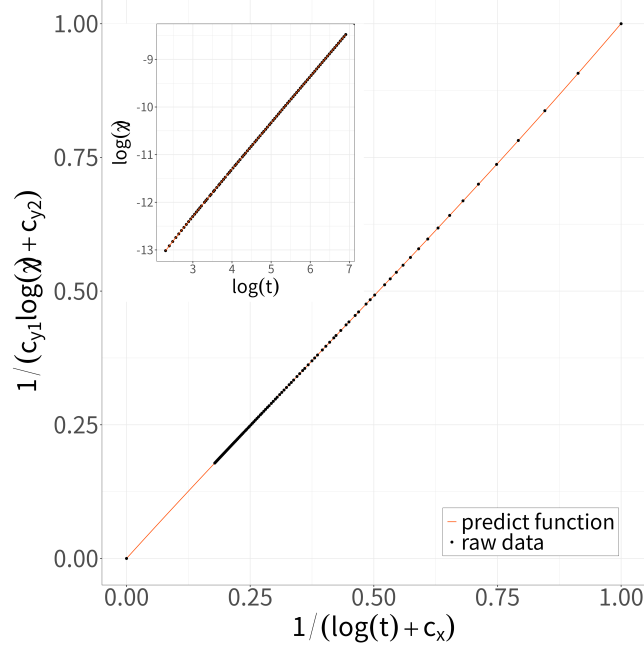


FIG. 14. (Color Online) Regression of $X = 1/(\log(t) + c_x)$ vs $Y = 1/(c_{y1} \log(\chi) + c_{y2})$ for the three-dimensional Ising model, within the bounds $0 \leq X, Y \leq 1$. Black closed circles represent raw data points from the simulation; the orange line depicts the interpolation. The inset shows the raw data of $\log(t)$ vs $\log(\chi)$ and their prediction.

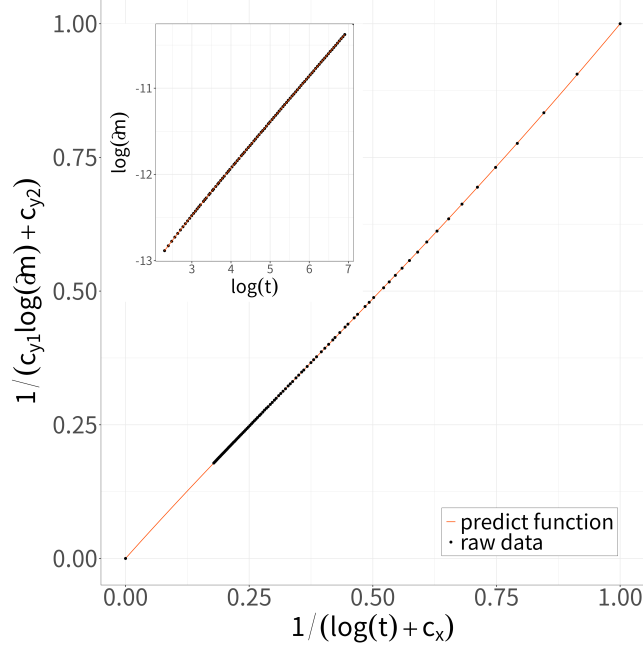


FIG. 15. (Color Online) Regression of $X = 1/(\log(t) + c_x)$ vs $Y = 1/(c_{y1}\log(\partial m) + c_{y2})$ for the three-dimensional Ising model, within the bounds $0 \leq X, Y \leq 1$. Black closed circles represent raw data points from the simulation; the orange line depicts the interpolation. The inset shows the raw data of $\log(t)$ vs $\log(\partial m)$ and their prediction.

Figures 16 to 19 display the interpolations of the local exponents, each plot has $N = 1003$ data points at equal intervals of t .

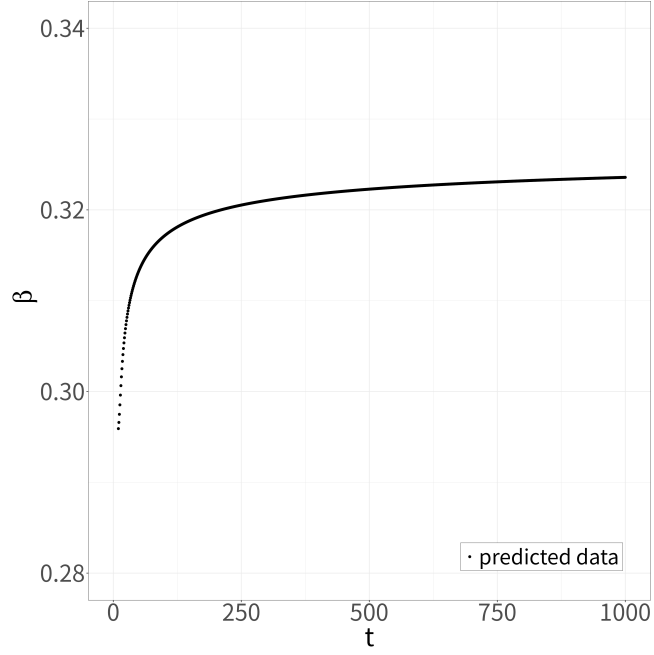


FIG. 16. Interpolation of t vs β for the three-dimensional Ising model. Black closed circles represent interpolated values at equal intervals of t .

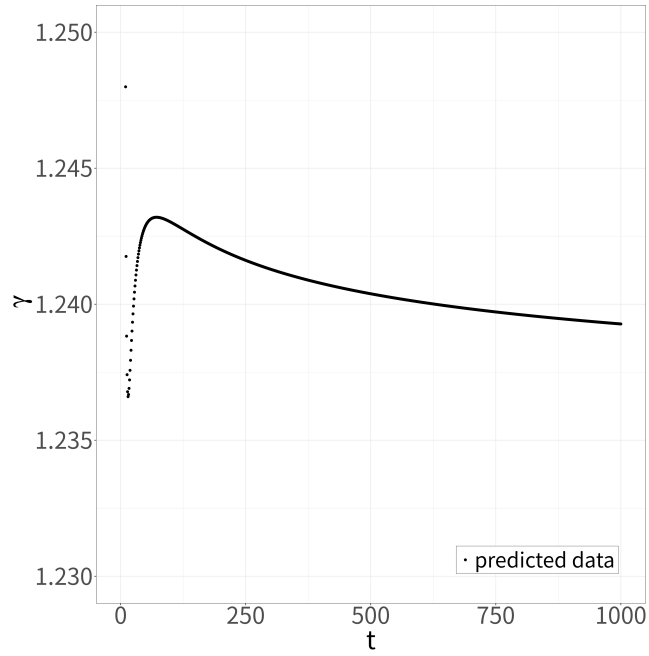


FIG. 17. Interpolation of t vs γ for the three-dimensional Ising model. Black closed circles represent interpolated values at equal intervals of t .

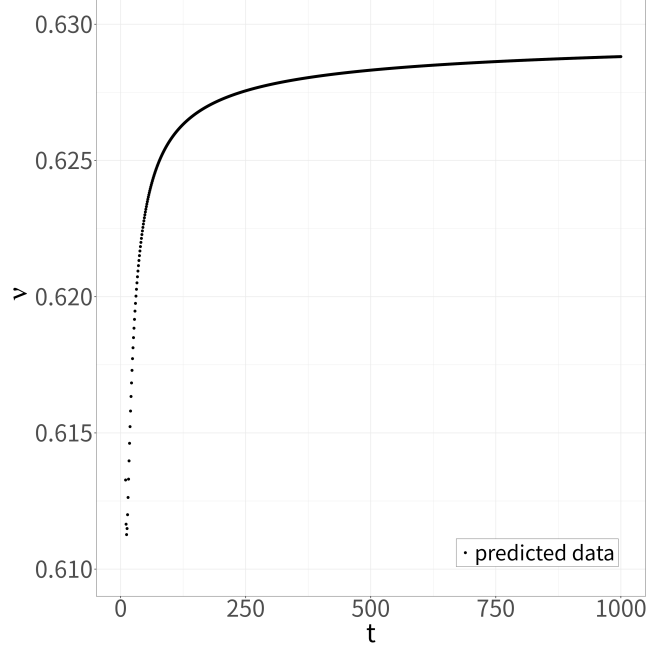


FIG. 18. Interpolation of t vs ν for the three-dimensional Ising model. Black closed circles represent interpolated values at equal intervals of t .

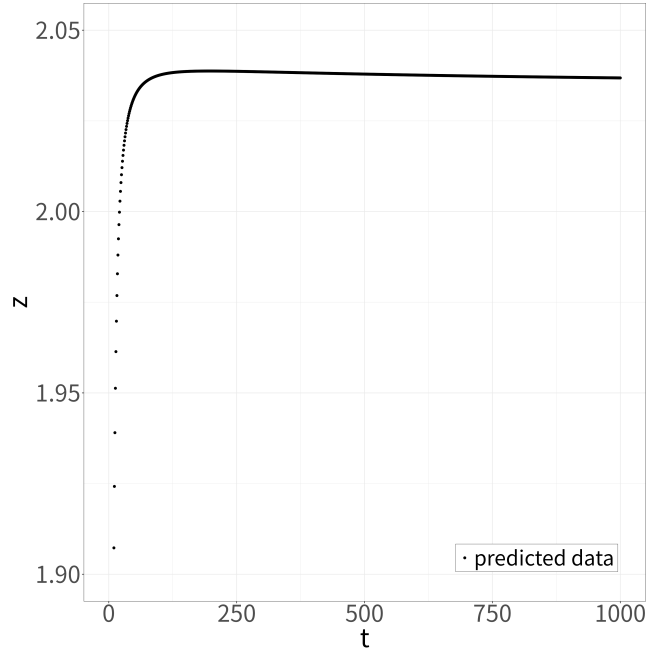


FIG. 19. Interpolation of t vs z for the three-dimensional Ising model. Black closed circles represent interpolated values at equal intervals of t .

Next, we perform the bootstrap method. We created 100 bootstrap samples by resampling

TABLE II. Critical exponents for the three-dimensional Ising model, as obtained from various studies.

Reference	Method	β	γ	ν	z
Ito <i>et al.</i> (2000) ^{3,29}	NER(at $T = 1/0.221660$)	0.325(5)		0.635(5)	2.055(10)
Butera and Comi (2002) ³⁰	High-temperature series		1.2371(1)	0.6299(2)	
Kos <i>et al.</i> (2016) ⁶	Conformal bootstrap			0.629971(4)	
Ron <i>et al.</i> (2017) ³¹	MC renormalization group	0.3250(2)	1.2356(8)	0.6285(4)	
Ferrenberg <i>et al.</i> (2018) ³²	MC		1.23708(33)	0.629912(86)	
Adzhemyan <i>et al.</i> (2022) ²⁸	ε expansion				2.0235(8)
Our results	NER(at $T = 1/0.2216547$)	0.3252(2)	1.2376(5)	0.6293(3)	2.0346(3)

$N_{\text{data}} = 100$ data points, which were extracted from the simulation data at equal intervals of $\log(t)$, 100 times. We applied the present method to each bootstrap sample independently and estimated the mean and numerical error of the critical exponents across bootstrap samples. Consequently, we estimated the critical exponents to be $\beta = 0.3252(2)$, $\gamma = 1.2376(5)$, $\nu = 0.6293(3)$, and $z = 2.0346(3)$. The results are shown in Table II. Compared with the results of the previous NER analysis,²⁹ our results show improved accuracy because of using a stable and automatic method with less influence of human bias. In the previous NER analysis, a large error bar was necessary because the reliability of convergence decreases due to discrete derivatives. However, it is considered that the previous analysis provided theoretically correct evaluations. The present method offers improvements that increase accuracy and reliability. Our results are close to those in other studies and would be improved if we used more accurate transition temperatures, a larger maximum observation time, or more samples. Nonetheless, because the present method estimates critical exponents close to the values found in previous studies, we consider it validated.

V. Summary and Discussion

We have improved the analysis of fluctuations in the NER method and have applied the present method to estimate critical exponents in both the two-dimensional square Ising

model and the three-dimensional cubic Ising model. The modifications include two significant advancements. First, we introduced the Gaussian process regression and transformed the physical quantities using Eq. (12). This transformation enables us to use the data point at $(X, Y) = (0, 0)$ as $t \rightarrow \infty$. As a result, we can reliably estimate the local exponents $\beta(t)$, $\gamma(t)$, $\nu(t)$, and $z(t)$ from simulation data. Second, under the assumption that these exponents converge exponentially, we extrapolated them using the ε -algorithm, which enabled systematic and reproducible extrapolation. The present method's automation and reproducibility reduce human bias, making it easier to apply the bootstrap method and provide statistical error estimates. Because the proposed method requires only the data of the relaxation of specific quantities from the Monte Carlo simulation, its simplicity imparts it with strong potential.

The results of our analysis are promising. For the two-dimensional Ising model, we obtained the critical exponents $\beta = 0.12504(6)$, $\gamma = 1.7505(10)$, and $\nu = 1.0003(6)$, which are consistent with the exact values. We obtained reliable $z = 2.1669(9)$ because of the high accuracy of these exponents; this value is consistent with that reported by Nightingale and Blöte.²⁶ The present method offers improvements in accuracy and reliability compared with the previous NER analysis that used discrete numerical derivatives. These results suggest that the present method is effective at the exact critical temperature. For the three-dimensional Ising model, we obtained the critical exponents $\beta = 0.3252(2)$, $\gamma = 1.2376(5)$, $\nu = 0.6293(3)$, and $z = 2.0346(3)$, which are close to the values reported in previous studies^{6,28,30–32} and improved accuracy compared with that achieved in the previous NER analysis.^{3,29} These results demonstrate the versatility of the present method and its potential applicability to various models. Although the results of the present method are not entirely consistent with those of previous studies, its significant advantage lies in its applicability to systems with slow relaxations, such as fully frustrated systems and those undergoing Kosterlitz–Thouless transitions. Therefore, the present method holds promise for analyzing difficult systems and contributing to research on the universality of critical phenomena.

Acknowledgments

The authors are grateful to Kazuaki Murayama for his valuable support and comments. The authors are grateful to the Supercomputer Center at the Institute for Solid State

Physics, University of Tokyo, for the use of their facilities.

* osada.yum@gmail.com

- ¹ Ozeki Y., Ito N., J. Phys. A, 1998, **31**, No. 24, 5451, doi:10.1088/0305-4470/31/24/007, URL <https://dx.doi.org/10.1088/0305-4470/31/24/007>.
- ² Ozeki Y., Ogawa K., Ito N., Phys. Rev. E, 2003, **67**, 026702, doi:10.1103/PhysRevE.67.026702, URL <https://link.aps.org/doi/10.1103/PhysRevE.67.026702>.
- ³ Ozeki Y., Ito N., J. Phys. A, 2007, **40**, No. 31, R149.
- ⁴ Harada K., Phys. Rev. E, 2011, **84**, No. 5, 056704, URL <https://journals.aps.org/pre/pdf/10.1103/PhysRevE.84.056704>.
- ⁵ Harada K., Phys. Rev. E, 2015, **92**, No. 1, 012106, URL <https://journals.aps.org/pre/pdf/10.1103/PhysRevE.92.012106>.
- ⁶ Kos F., Poland D., Simmons-Duffin D., Vichi A., J. High Energy Phys., 2016, **2016**, No. 8, 36, URL [https://link.springer.com/article/10.1007/JHEP08\(2016\)036](https://link.springer.com/article/10.1007/JHEP08(2016)036).
- ⁷ Levin M., Nave C. P., Phys. Lett., 2007, **99**, No. 12, 120601, URL <https://journals.aps.org/prl/abstract/10.1103/PhysRevLett.99.120601>.
- ⁸ Berezinskii V., Sov. Phys. JETP, 1971, **32**, No. 3, 493–500, URL <https://inspirehep.net/files/f55503250f690969aedfda4ceaf9b4f9>.
- ⁹ Berezinskii V., Sov. Phys. JETP, 1972, **34**, No. 3, 610–616, URL <https://inspirehep.net/files/0f7b50c47ec26bed99a50ff199960259>.
- ¹⁰ Kosterlitz J. M., Thouless D. J., J. Phys. C: Solid State Phys., 1973, **6**, No. 7, 1181, doi:10.1088/0022-3719/6/7/010, URL <https://dx.doi.org/10.1088/0022-3719/6/7/010>.
- ¹¹ Kosterlitz J. M., J. Phys. C: Solid State Phys., 1974, **7**, No. 6, 1046, doi:10.1088/0022-3719/7/6/005, URL <https://dx.doi.org/10.1088/0022-3719/7/6/005>.
- ¹² Ozeki Y., Matsuda A., Echinaka Y., Phys. Rev. E, 2019, **99**, No. 1, 012116, URL <https://journals.aps.org/pre/pdf/10.1103/PhysRevE.99.012116>.
- ¹³ Ozeki Y., Yotsuyanagi S., Sakai T., Echinaka Y., Phys. Rev. E, 2014, **89**, No. 2, 022122, URL <https://journals.aps.org/pre/pdf/10.1103/PhysRevE.89.022122>.
- ¹⁴ Terasawa Y., Ozeki Y., J. Phys. Soc. Japan, 2023, **92**, No. 7, 074003.

- ¹⁵ Ozeki Y., Yajima Y., Nakamura Y., Phys. Rev. B, 2020, **101**, No. 9, 094437, URL <https://journals.aps.org/prb/pdf/10.1103/PhysRevB.101.094437>.
- ¹⁶ Osada Y., Ozeki Y., J. Phys. Soc. Japan, 2023, **92**, No. 8, 084004, URL <https://journals.jps.jp/doi/full/10.7566/JPSJ.92.084004>.
- ¹⁷ Echinaka Y., Ozeki Y., Phys. Rev. E, 2016, **94**, 043312, doi:10.1103/PhysRevE.94.043312, URL <https://link.aps.org/doi/10.1103/PhysRevE.94.043312>.
- ¹⁸ Ito N., Pramana J. Phys., 2005, **64**, 871–880, URL <https://link.springer.com/content/pdf/10.1007/BF02704149.pdf>.
- ¹⁹ Nakamura T., Phys. Rev. E, 2016, **93**, No. 1, 011301, URL <https://journals.aps.org/pre/pdf/10.1103/PhysRevE.93.011301>.
- ²⁰ Nakamura T., Sci. Rep., 2020, **10**, No. 1, 14201, URL <https://www.nature.com/articles/s41598-020-70389-0>.
- ²¹ Johnson J. E., Laparra V., Pérez-Suay A., Mahecha M. D., Camps-Valls G., PloS one, 2020, **15**, No. 10, e0235885, URL <https://journals.plos.org/plosone/article?id=10.1371/journal.pone.0235885>.
- ²² Wynn P., Math. Tables Aids Comput., 1956, **10**, No. 54, 91–96, URL <http://www.jstor.org/stable/2002183>.
- ²³ Sidi A., Practical Extrapolation Methods: Theory and Applications, Cambridge University Press, 2003, URL <https://www.cambridge.org/core/books/practical-extrapolation-methods/21A93C2B0793CF09B2F3ABEF78F3F9B9>.
- ²⁴ Brezinski C., Redivo-Zaglia M., Extrapolation and Rational Approximation, Springer, 2020, URL <https://link.springer.com/book/10.1007/978-3-030-58418-4>.
- ²⁵ Shanks D., J. Math. Phys., 1955, **34**, No. 1-4, 1–42, URL <https://onlinelibrary.wiley.com/doi/abs/10.1002/sapm19553411>.
- ²⁶ Nightingale M., Blöte H., Phys. Rev. B, 2000, **62**, No. 2, 1089, URL <https://journals.aps.org/prb/abstract/10.1103/PhysRevB.62.1089>.
- ²⁷ Efron B., Ann. Statist., 1979, **7**, No. 1, 1 – 26, doi:10.1214/aos/1176344552, URL <https://doi.org/10.1214/aos/1176344552>.
- ²⁸ Adzhemyan L. T., Evdokimov D., Hnatič M., Ivanova E., Kompaniets M., Kudlis A., Zakharov D., Phys. Lett. A, 2022, **425**, 127870, URL <https://www.sciencedirect.com/science/article/abs/pii/S0375960121007349>.

- ²⁹ Ito N., Hukushima K., Ogawa K., Ozeki Y., J. Phys. Soc. Japan, 2000, **69**, No. 7, 1931–1934, URL <https://journals.jps.jp/doi/abs/10.1143/JPSJ.69.1931>.
- ³⁰ Butera P., Comi M., Phys. Rev. B, 2002, **65**, No. 14, 144431, URL <https://journals.aps.org/prb/abstract/10.1103/PhysRevB.65.144431>.
- ³¹ Ron D., Brandt A., Swendsen R. H., Phys. Rev. E, 2017, **95**, No. 5, 053305, URL <https://journals.aps.org/pre/abstract/10.1103/PhysRevE.95.053305>.
- ³² Ferrenberg A. M., Xu J., Landau D. P., Phys. Rev. E, 2018, **97**, No. 4, 043301, URL <https://journals.aps.org/pre/abstract/10.1103/PhysRevE.97.043301>.